SimBuild
2024

Eleventh National Conference of IBPSA-USA
Denver, Colorado
May 21 – 23, 2024

Hygrothermal Behavior of 3D Concrete Printed Wall Assemblies

Ehsan Ghaderi[1], Pete Evans[1], Shelby Doyle[1], Nick Senske[1], and Chengde Wu[1]
[1]Iowa State University, Ames, IA

Abstract

The rapid development of 3D concrete printing technology has brought significant advancements to the construction industry. However, the hygrothermal behavior of 3D concrete printed walls remains an understudied area despite its critical implications for building durability and performance. This study explores the hygrothermal performance of 3D concrete printed wall assemblies, focusing on moisture accumulation, frost damage, mold growth, and corrosion risks. Employing the WUFI 2D simulation tool, we compare various insulation materials, concrete types, and wall designs to identify the most effective wall assemblies for 3D concrete printing. The findings indicate that cellulose insulation, due to its higher moisture content, is less suitable for 3D concrete printed walls, posing a higher risk of frost damage. Conversely, insulation materials with higher density and vapor resistance demonstrate better hygrothermal performance. The wall assembly with a layer of concrete bead connecting the interior and the exterior concrete layers leads to higher water content. Moreover, varying levels of vapor resistance in different concrete types affect the overall drying capability. Despite high relative humidity levels, no visible mold growth is predicted in the simulated assemblies, suggesting adequate mold resistance in the wall assemblies.

Introduction

3D concrete printing (3DCP) offers many appealing features, such as design freedom in curved geometries, automating construction process, and so on. However, there are many challenges in 3DCP, such as hardware design, software workflow (Wu et al. 2024), material mix, carbon footprint, energy performance (Wu et al. 2023), etc. The hygrothermal analysis assesses a building's response to moisture and temperature over time, enhancing understanding of its envelope's performance and highlighting potential issues (Glass et al. 2013). The hygrothermal behavior of 3DCP walls is also not well known (Pessoa et al. 2023). Moisture-related issues in building assemblies can be the root of several issues and can be categorized as visible and invisible degradations (ASHRAE 2021). Invisible degradation reduces the thermal resistance of buildings and insulations and the load-bearing capacity of materials. Visible degradation is related to mold growth, decay of wooden materials, frost damage, corrosion of metals, damage from expansion of materials, hydration of plastics, and effect on appearance (ASHRAE 2021).

There are numerous advantages to hygrothermal studies, including:

- Hygrothermal simulation aids in understanding moisture and temperature conditions within a building envelope (Glass et al. 2013).
- It helps determine the suitability of a building envelope design for a specific climate.
- Moisture issues, which are expensive to rectify post-construction, often result from construction flaws, building operation, incorrect maintenance, and improper design (Glass et al. 2013).
- In recent decades, hygrothermal models have been developed to study the coupled effects of heat and moisture (Delgado et al. 2010).
- While not always necessary, hygrothermal simulation is increasingly important due to industry changes, new technologies, and construction techniques, aiding in the prediction of moisture performance for new building materials and assemblies.

Hygrothermal performance is based on being either fail or pass (TenWolde, 2011) and serves a dual purpose, as they not only aid in decision-making during the design process but also provide valuable insights for evaluating the performance of existing buildings and retrofits and restoration projects (ASTM, 2023). Hence, investigating the hygrothermal characteristics of 3DCP wall assemblies can be highly beneficial due to the novelty of this technology, the limited availability of projects to observe its performance, and the lack of sufficient empirical data regarding the utilization of 3D concrete printing. While extensive research has been conducted in North America on wooden envelopes, there is little research on the moisture behavior of 3DCP assemblies.

Research Questions

- What is the possibility of mold growth in 3D-printed concrete (3DCP) Wall Assemblies?
- How do different insulation types affect the hygrothermal behavior of the 3DCP walls?
- What characteristics of 3DCP walls affect hygrothermal behavior?

Research Goals

This study investigates the hygrothermal behavior of 3D-printed concrete walls, including drying time, moisture accumulation, frost damage, corrosion of metals, and the possibility of mold growth. In addition, comparing different insulation types, the most effective Wall Assembly for 3D printing concrete based on the results of the hygrothermal simulations in a certain climate condition is identified.

Research MethodologyThe primary research method employed in this study is computer simulation, utilizing WUFI 2D version 4.4 for the simulation of two-dimensional transient heat and moisture transfer. WUFI is a tool widely recognized for its ability to analyze the hygrothermal behavior of building components. In this research, we focused on designing three different types of 3DCP walls to investigate their hygrothermal performance, particularly examining aspects such as drying time and water accumulation.

Background

Mold grows in building components under certain circumstances. Some molds threaten human health and can affect individuals differently, and it is necessary to reduce the favorable conditions for mold growth in buildings (Krus et al. 2007). Several mold growth prediction models have been developed based on laboratory tests, including the VTT model, a mathematical model of mold growth proposed by Hukka and Viitanen (Hukka and Viitanen, 1999), Isopleth model, and Biohygrothermal model, and they primarily rely on the interplay between temperature and relative humidity (Vereecken et al. 2015). For the purposes of this research, we will focus on the VTT model.

The VTT mold growth model is an empirical model (Glass et al. 2017) based on the favorable conditions for mold growth and is experimentally validated based on visual findings of mold growth (Viitanen et al. 2015). The model utilizes an index from zero to six (no mold to 100 percent mold coverage), highlighting the intensity of mold growth. The VTT model considers four sensitivity classes: very sensitive, sensitive, medium resistant, and resistant based on the materials' sensitivity to mold growth. It also contains the decline factor (which means reducing the mold index) whenever the conditions do not favor mold growth (Ojanen et al. 2010). AHSRAE 160 recommendations adopted the VTT model (Lepage et al. 2019), requiring the index to stay below three. WUFI VTT is a postprocessor based on the VTT model, which uses a traffic light system to aid in assessing the risk of mold growth: green signifies no risk, red denotes an unacceptable condition, and yellow suggests a potential risk that necessitates further evaluation (Viitanen et al. 2015).

Thermal insulation also impacts the moisture behavior of wall assemblies. Insulation and generally any building component with different moisture transport characteristics, if not applied appropriately, can result in unfavorable hygrothermal behavior. External insulation is typically perceived as the more secure choice, offering effective shielding against the external environment (Jensen et al. 2020). In contrast, internal insulation, which is common in retrofitting and renovating, is considered riskier since it does not protect the exterior part of the assembly and can reduce the drying capability (Straube and Schumacher 2007).

Additionally, attachment mechanisms such as metal components can face corrosion under high humidity or certain conditions; for instance, metal fasteners in wooden assemblies can corrode due to the organic acids in the wood (Zelinka 2013). In concrete, due to the carbonated coverage of steel, corrosion happens at above 80% relative humidity, while steel corrodes in humidity above 60% (Künzel et al. 2008). ASHRAE 160 requirements for corrosion suggest that the threshold should be derived from the metal characteristics, and if such information is not provided, the 30-day hourly average of the metal surface humidity should stay under 80% (ASHRAE 160 2021).

Water in porous materials can freeze, and this phase change threatens the material in several manners, including structural strength, cracks, and visual appearance. Concrete, as a porous building component, has relatively high moisture storage capabilities, and during cold weather, when the temperature falls below 32 degrees Fahrenheit (0 degrees Celsius), the trapped moisture can freeze. Li et al. observed frost damage in specimens with 86-88% degree of saturation (corresponds to 98% relative humidity) during the freeze-thaw cycles and found that while increasing air content can delay the time to reach that degree of saturation, it does not impact the frost damage (Li et al. 2012). WTA (Wissenschaftlich - Technische

Arbeitsgemeinschaft für Bauwerkserhaltung und Denkmalpflege, translates to "Scientific and Technical Working Group for Building Maintenance and Monument Preservation") guideline recommends 95% relative humidity as the threshold for frost damage in frost susceptible materials and free saturation (corresponds to 100% relative humidity) for frost-resistant materials, including concrete (WTA, 2012).

Simulations

Modeling Technique

Several mathematical methods have been developed to predict the moisture behavior of building envelopes (Straube and Burnett 2001). WUFI, DELPHIN, and HygIRC are computer software programs frequently used for hygrothermal analysis. WUFI is a one- or two-dimensional computer program for transient heat and moisture transport developed by the Fraunhofer Institute in Building Physics located in Stuttgart, Germany. This simulation tool is extensively used and validated by laboratory tests (Glass and TenwWolde 2017, Overton 2019, Glass et al. 2015, Straube and Schumacher 2006). WUFI stands for Wärme-und Feuchtetransport instationär, which translates in English to "Transient Heat and Moisture Transport." WUFI provides moisture performance and damage assessment of the building envelopes, including drying time and water accumulation (Yu et al. 2016). ASHRAE 160 requirements for mold are embedded in the WUFI Mold Index VTT software add-on. WUFI pro, which is one-dimensional, has modeling limitations and cannot define complex geometries. Since the 3D-printed concrete wall section cannot be modeled using the one-dimensional tool, the following research is conducted using WUFI 2D version 4.4. In WUFI 2D, geometries need to be represented using only rectangular shapes. Figure 1 shows the discretized model of a 3D concrete printed wall Assembly with non-rectangular shapes.

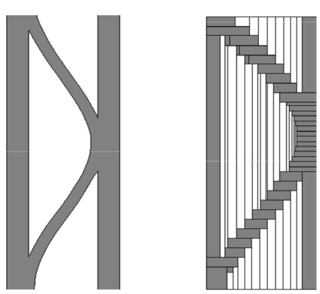

Figure 1 The standard 3DCP wall 3DCP section (A) and The modified 3DCP wall section geometry in WUFI (B)

Wall Assemblies and Materials

Figure 2 shows the three Wall Assemblies simulated in WUFI 2D in this study. The material properties of the 3DCP Wall Assemblies were taken from the WUFI database, as shown in table 1.

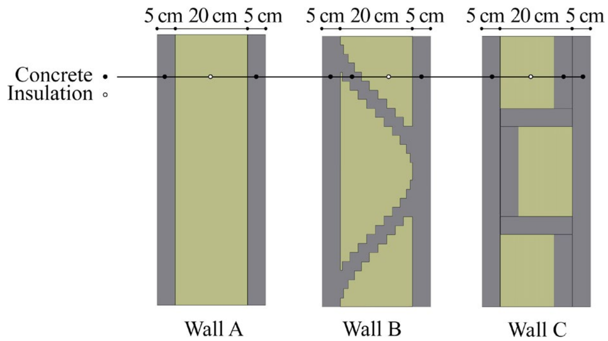

Figure 2 3DCP Wall Assemblies

Table 1 Material properties

Material	Bulk density	Porosity	Heat Capacity	Thermal Conductivity	Vapor resistance
	kg/m³	m³/m³	J/KgK	W/mK	
Concrete C12/15	2200	0.18	850	1.6	92
Concrete C35/45	2200	0.18	850	1.6	248
Concrete w/c= 0.5	2300	0.18	850	1.6	180
Cellulose Fiber Insulation	30	0.99	1880	0.036	1.86
Fiberglass	30	0.99	840	0.035	1.3
Rockwool CAVITYROCK®	73	0.95	850	0.032	1.1
Sprayed foam closed cell	39	0.99	1470	0.025	88.93

Simulation settings

The weather data of Des Moines, Iowa, in climate zone 5A, was used as the outdoor condition. The weather data in WUFI shows that the Southeast has the most wind-driven rain, and the North side always has the lowest sun exposure. To identify the worst-case scenario, the concrete used in the simulation is set to C35/45 (meaning 28-day compressive strength between 35 - 45 MPa), and the insulation is set to cellulose for both the north and southeast walls (figure 3). Results suggest that the total water content of the SE direction is considerably higher than the N direction. Therefore, SE is chosen as the wall direction for all following simulations.

Rain load calculation is set according to ASHRAE standard 160 for building heights less than 10 meters and walls below a steep-slope roof. The exposure category is set to medium. Default values for surface transfer coefficients (exterior and interior sides) were selected as specified in Table 2.

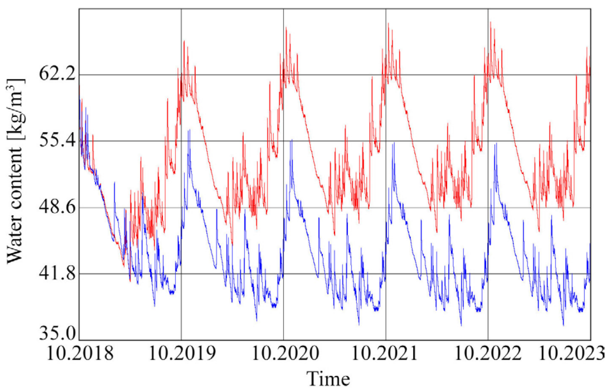

Figure 3 Total water content of Wall A in Both N (blue) and SE (red) direction

ASHRAE 160-2021 suggests that the moisture year for hygrothermal studies should be the second-highest severe year of 30-year weather data. Therefore, ASHRAE Year 2, the second most severe year out of 10 years, was selected for the outdoor climate.

The ASHRAE model is selected for the indoor surface. The indoor design humidity intermediate method based on ASHRAE recommendations is used. In this method, indoor design humidity is determined by hourly weather, and the effect of the HVAC system is considered. The default set point of 21.1 °C for heating and 23.9 °C for cooling was selected. Air-Conditioning was selected as the A/C type. The number of bedrooms was set to two (three occupants), and the air exchange rate to 0.2 as standard construction to satisfy ASHRAE 160, which considers moisture generated by occupants. The building volume is assumed to be 500 cubic meters.

WUFI Initial conditions

ASHRAE standard 160 suggests that the initial moisture content for hygrothermal simulations of new constructions should be two times the equilibrium moisture content at 90% humidity (EMC90) for concrete and two times EMC80 for other materials. This standard allows lower initial moisture content if construction materials and the construction process are protected from high relative humidity and moisture exposure, and the EMC90 for concrete and EMC80 for other materials can be applied (ASHRAE 160 2021). In this study, the initial moisture content is set to two times the EMC90 for concrete (supersaturated) and two times EMC80 for other materials. The initial temperature is not an important factor since the temperature of the assembly components will quickly adapt to the boundary conditions. The initial temperature is set to the default of 20 °C.

To assess hygrothermal simulations, both the moisture behavior of the assembly during the first years of the simulation and the hygrothermal conditions after reaching the dynamic equilibrium need to be considered (Kaczorek 2018). Therefore, the simulation duration should be long enough to reach the dynamic equilibrium of seasonal changes. Based on the ASHRAE standard 160 recommendations, this study considers five years (43800 hourly steps) as the simulation time steps for Wall A. However, due to the long simulating duration and WUFI 2D limitations, walls B and C are simulated for four years (35100 hourly steps). According to ASHRAE standard 160, the maximum total moisture content of the assembly in the final year of the simulation shall be equal to or less than that of the prior year (ASHRAE 160 2021). The simulation period starts on October 1st, 2018, at 00:00 am at "hourly" resolution with adaptive time step control enabled (which reduces the simulation errors by adapting each time step result to the previous one). One percent fraction of rain load is considered on the exterior layer of the insulation according to ASHRAE 160 recommendations. Table 2 shows the summary of the WUFI initial conditions.

Table 1 input parameters

Climate = Des Moines, Iowa	Climate data = Year 2	
Azimuth = 270	Orientation = Southeast	Inclination = 90°
Rain load = ASHRAE 160	Building Height < 10 m	Exposure category = Medium
Exterior Surface		
Heat transfer Coefficient = 17	Short-Wave Radiation absorptivity = 0.2	Long-Wave Radiation Emissivity = 0.9
Sd-value = 0	Adhering fraction rain = Depending on the inclination of the component.	
Interior Surface		
Heat transfer Coefficient = 8	Sd-value = 0	AC type = Air conditioning
Floating indoor temperature shift = 2.8°	Heating set point = 21.1°	Cooling set point = 23.9°
Number of bedrooms = 2	Air exchange rate = 0.2	Building volume = 500 m³
The adaptive time step control is enabled.	Steps = 3	Max stages = 5

Discussion and result analysis

Comparison by insulation material

In order to study the impact of different insulations on the hygrothermal behavior of the 3D printed concrete walls, Wall A is simulated with four common insulation materials: Cellulose fiber, Fiberglass, Sprayed foam closed cell, and Rockwool Cavityrock. The simulation results of water content, mold index, corrosion, and frost are summarized below:

1. Water content

   Figure 4 shows the total water content (TWC) for Wall A with different insulations. Results suggest that the TWC of the wall with cellulose is higher than all other insulations, and over five years, water is still slightly accumulating and does not reach equilibrium. Besides, the initial water content does not dry off for the duration of the simulation. The overall water content for Rockwool, Fiberglass, and Sprayed foam insulations has similar trends, and the initial water content dried off after the first few months. Wall A with Rockwool, Fiberglass, and Sprayed Foam reaches the annual trend in the first year, the initial water content dries off, and no water accumulation is observed.

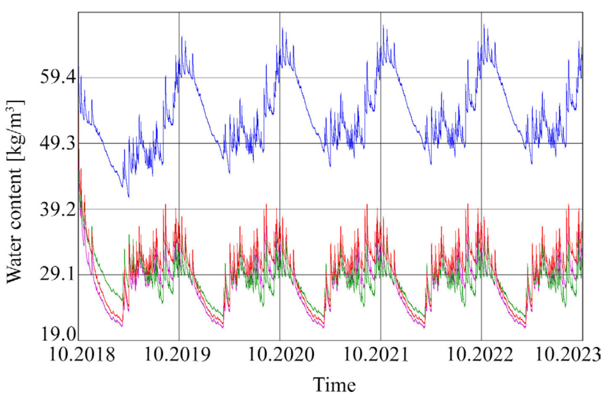

Figure 4 Total water content of Wall A C35/45 with Cellulose (blue), Fiberglass (red), Spray foam (green), and Rockwool (purple) as insulation.

2. Mold index

   The WUFI Mold Index VTT add-on is used to study the possibility of mold growth in Wall A with different insulations since this add-on includes the ASHRAE requirements. Three monitor points inside the wall assembly are chosen to evaluate the mold index: the interior face of the inner concrete layer, the intersection of the insulation and the inner concrete layer, and the middle of the insulation (Figure 5). The exterior layers are not taken into account since mold growth models are not developed for the exterior layers of the assemblies. These parts are mostly under the influence of outside conditions, which are difficult to model accurately and consider in the simulation.

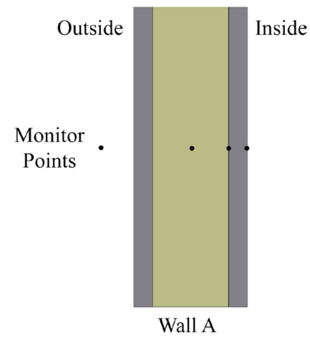

Figure 5 Mold growth monitor points in 3DCP Wall A

Since the interior surface of the Wall Assembly is in direct contact with the ambient air, the sensitivity class is set to very sensitive. For the other monitoring point, the sensitivity class is set to medium resistant. The VTT model takes into account the decrease in mold index when the condition is unfavorable for mold growth. The decline factor of mold is set to a relatively low decline (0.25) to be more conservative and have a more critical condition for simulations. Table 3 shows the mold index at the three monitor points. Figures 6 to 8 are mold index graphs for each monitor point.

Table 2 Mold index at monitor points

Monitor point	**Mold Index**			
	Rock-wool	**Spray Foam**	**Fiber-glass**	**Cellulose**
Inner concrete layer interior face	0.462	0.523	0.451	0.286
Intersection: insulation - inner concrete layer	0.138	0.145	0.091	0.061
Insulation Center	0.339	0.276	0.319	0.136

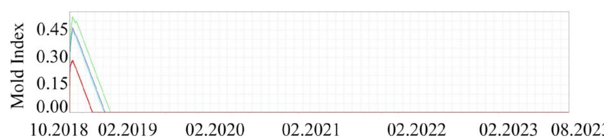

Figure 6 Mold index of the interior surface of the inner concrete layer. Cellulose (red), Rockwool (blue), Sprayed foam (green), and Fiberglass (cyan).

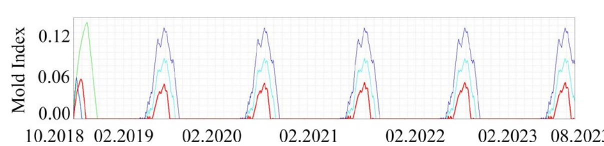

Figure 7 Mold index of the intersection of insulation and the inner concrete layer. Cellulose (red), Rockwool (blue), Sprayed foam (green), and Fiberglass (cyan).

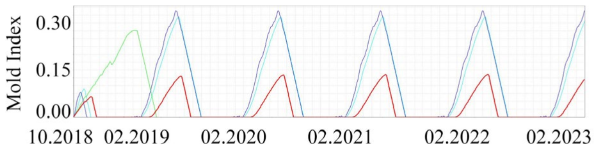

Figure 8 Mold index of the middle of insulation. Cellulose (red), Rockwool (blue), Sprayed foam (green), and Fiberglass (cyan).

In all three monitor positions, the mold index remains below three, which indicates no visible mold on the surface of materials and satisfies the requirement of ASHRAE 160. The mold index of the insulation and exterior concrete layer intersection has an incremental trend.

3. Corrosion

Figure 9 shows the 30-day hourly average relative humidity at the intersection of the insulation and the exterior concrete layer in Wall A with four types of insulations. According to ASHRAE 160 recommendations, to avoid corrosion, the 30-day hourly average RH should not exceed 80%. However, for all four assemblies of Wall A, relative humidity is above 91%, and the corrosion of metal components is expected. This high relative humidity can be due to the moisture transport resistance of the insulation layer and the high moisture exposure of the exterior concrete layer.

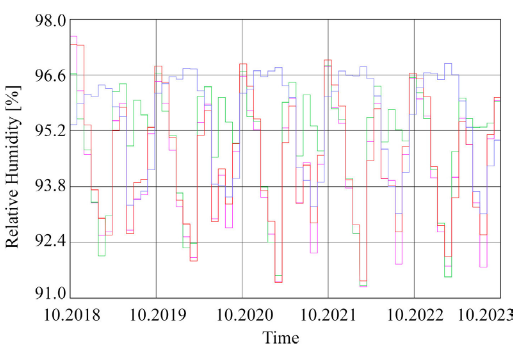

Figure 9 30-day hourly average relative humidity of the intersection of the exterior concrete layer and the insulation in Wall A with C35/45 concrete, and Cellulose (blue), Fiberglass (red), Sprayed foam (green), and Rockwool (purple) as insulation

4. Frost

Figures 10 to 13 show the graphs of relative humidity and temperature for Wall A with the four insulations at the exterior concrete layer. The results show that Wall A with cellulose has considerable frost damage risk since relative humidity is above 95% when the temperature is below zero Celsius most of the time in the cold season (see Figure 10). In Wall A with fiberglass, there are a few occasions where the relative humidity is over 95% when the temperature is below zero Celsius (see Figure 11). Wall A with sprayed foam shows rare surpassing the frost damage threshold, indicating a secure option in case of frost damage risk (see Figure 12). In Wall A with Rockwool, a minor exceeding of 95% RH happens when the temperature is freezing (see Figure 13). Therefore, sprayed foam closed cell is the safest choice among all insulation types regarding the frost damage risk.

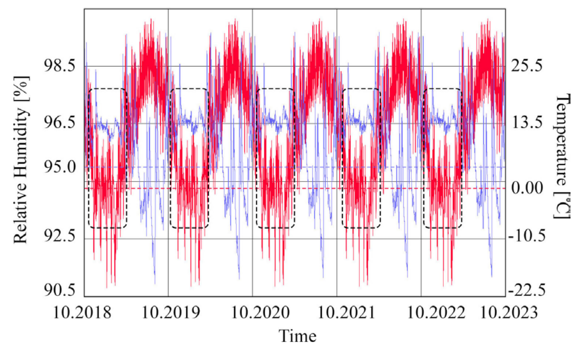

Figure 10 Humidity (blue) and temperature (red) for Wall A with cellulose at exterior concrete layer.

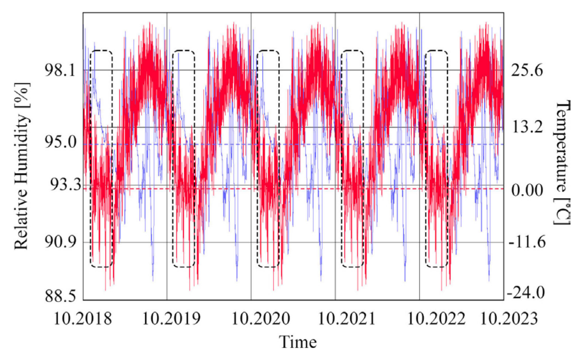

Figure 11 Humidity (blue) and temperature (red) for Wall A with Fiberglass at exterior concrete layer.

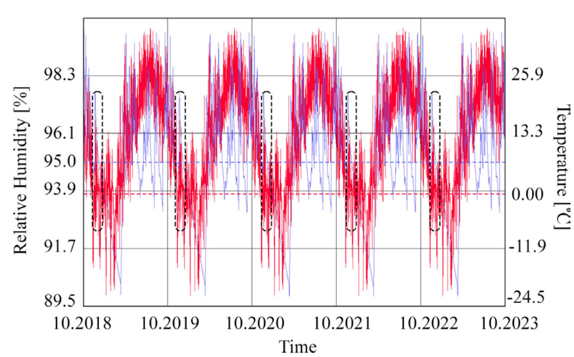

Figure 12 Humidity (blue) and temperature (red) for Wall A with Sprayed Foam at exterior concrete layer.

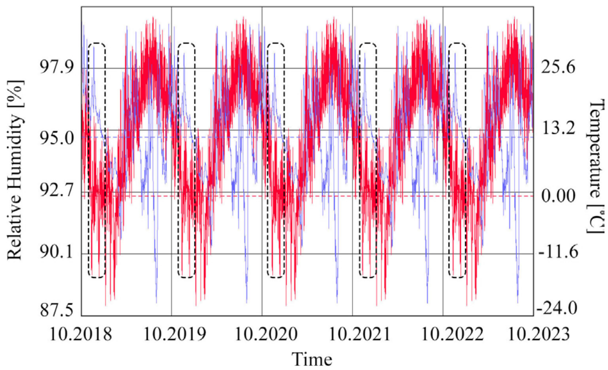

Figure 13 Humidity (blue) and temperature (red) for Wall A with Rockwool at exterior concrete layer.

Comparison of different Wall Designs

1. Water Content

C35/45 is chosen as the concrete, and Rockwool Cavity rock as the insulation to compare the hygrothermal behavior of Wall A, Wall B, and Wall C. Figure 14 shows the total water content of these Wall Assemblies. The total water content of Wall A is the lowest, and Wall C is considerably higher than the other two. We speculated that the concrete connection between the exterior and interior concrete layers increases in moisture transport due to concrete's higher moisture transport capabilities than insulations. Water can move through the concrete bridge between the two layers and increase the water level of the Wall Assembly.

All three assemblies reach the annual trend in the first year, and the initial water content of the walls dries in the first few months. Wall A, since it has no bridge between the interior and exterior concrete layers, has the lowest water content

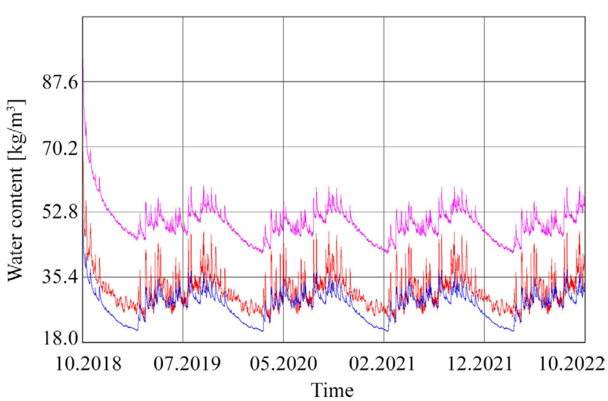

Figure 14 Total water content of Wall A in blue, Wall B in red, and Wall C in purple.

2. Mold Index

Table 4 shows that the mold index of all three wall designs stays below 3.0, as recommended in ASHRAE 160. Figures 15 and 16 show the mold index graphs of these assemblies. The mold index reaches zero after the drying of initial moisture in the first year for the interior face of the inner concrete layer in all three walls. At the intersection of insulation and the inner concrete layer, the mold index has a yearly cycle. However, it never surpasses the threshold of three (Wall B and Wall C are simulated for a duration of four years, while Wall A simulated for five years).

Table 3 Mold index of different wall types.

Monitor point	Mold Index		
	Wall A	**Wall B**	**Wall C**
The interior face of the inner concrete	0.524	0.456	0.71
The intersection of the insulation and the inner concrete layer	0.125	0.091	0.214

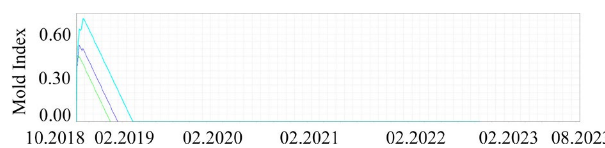

Figure 15 Mold index of the interior face of the inner concrete. Wall A is blue, Wall B is green, and Wall C is cyan.

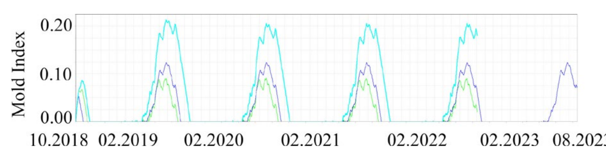

Figure 16 Mold index of insulation and inner concrete intersection. Wall A is blue, Wall B is green, and Wall C is cyan.

3. Corrosion

Figure 17 shows the 30-day hourly average relative humidity at the intersection of the insulation and the exterior concrete layer in Wall A, Wall B, and Wall C. Results show that the 30-day hourly average relative humidity is higher than 87%, which is more than the 80% threshold according to ASHRAE 160. Hence, steel members added to 3D-printed concrete may corrode.

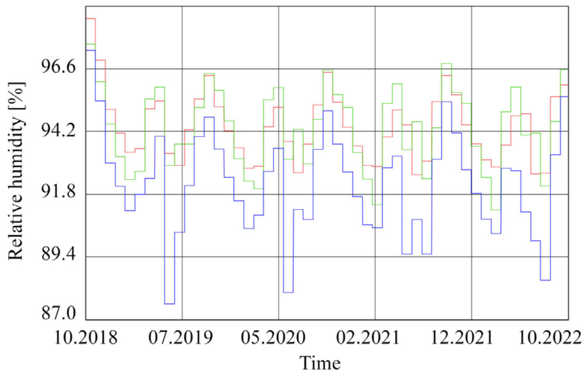

Figure 17 30-day hourly average Relative humidity at the exterior concrete layer and insulation intersection in Wall A (green), Wall B (blue), and Wall C (red).

4. Frost

   Figures 18 to 20 show the graphs of relative humidity and temperature for Wall A, Wall B, and Wall C. C35/45 is selected as the concrete, and Rockwool is the insulation in all these assemblies. Results suggest minimal incidents where relative humidity exceeds 95% when the temperature is lower than zero Celsius.

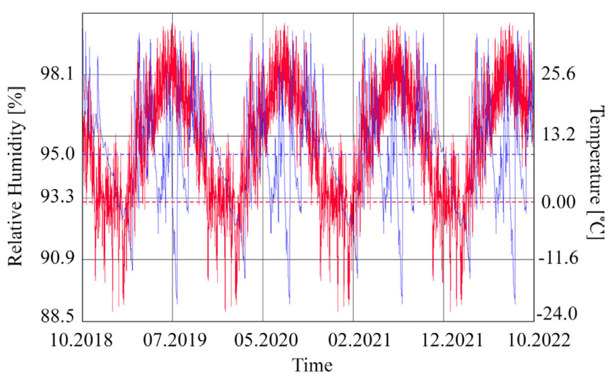

Figure 18 Relative humidity (blue) and temperature (red) for Wall A at the exterior concrete layer.

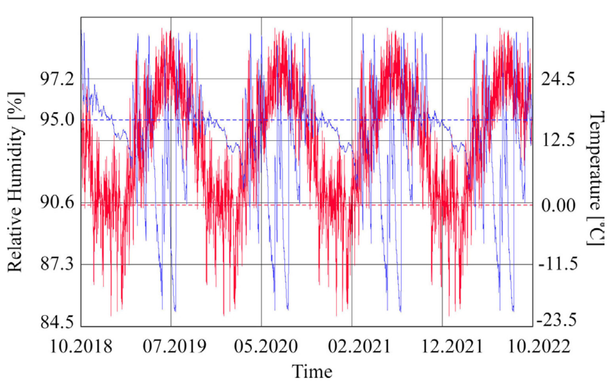

Figure 19 Relative humidity (blue) and temperature (red) for Wall B at the exterior concrete layer.

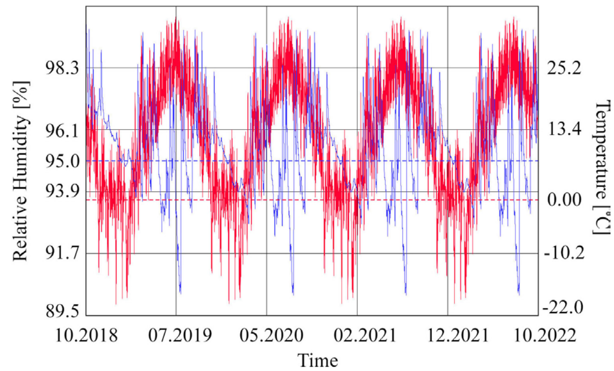

Figure 20 Relative humidity (blue) and temperature (red) for Wall C at the exterior concrete layer.

Comparison of different concrete types

1. Water Content

   Wall B was studied with three concretes from the WUFI database to evaluate the effect of different concretes on the hygrothermal behavior of 3DCP. Based on the WUFI database, the major difference in the characteristics of concretes is in vapor resistance. Concrete C35/45 has the highest (248), "W/C=0.5" is the next (180), and C12/15 has the lowest vapor resistance (92). Figure 21 shows the water content of each assembly.

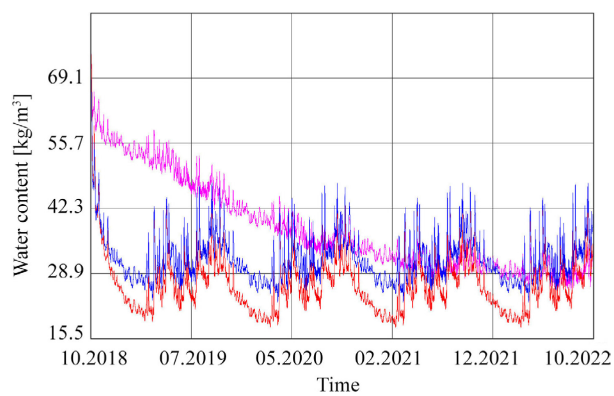

Figure 21 Total water content of Wall B with different concretes.

Results suggest that Wall B with C12/15 concrete has the lowest water content level and dries faster. Wall B with C35/45 and C12/15 reaches the annual trend in the first year, and the initial water content dries off in the first few months. "W/C=0.5" concrete does not reach the annual trend in a 4-year simulation, and the drying time of the initial moisture content is considerably high and stays considerably higher in the first two years. However, the moisture content of this assembly dries for the simulation duration and is comparable to the other assemblies in the last two years.

The water content of the insulation layer for different concrete types is shown in Figure 22. The water content of the insulation layer of the wall with "W/C=0.5" concrete is much higher than C35/45 and C12/15 in the first two years, and it has an incremental trend in the first months of the simulation. However, the insulation water content dries off in the third year.

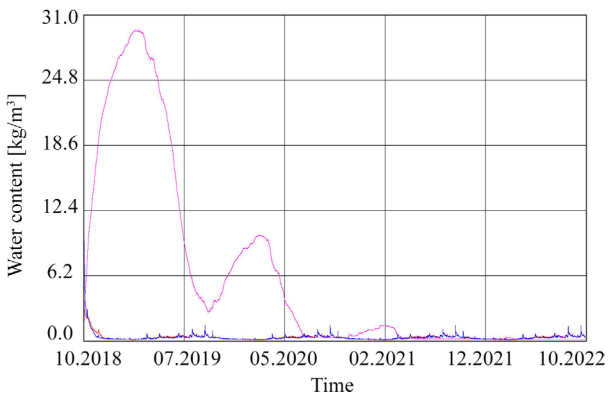

Figure 22 Water content of insulation layer in Wall B.

The inner concrete layer's water content of the wall with C12/15 concrete is lower than the two others, and the wall with "W/C=0.5" concrete has the highest in the first years, resulting in a longer drying time (figure 23). In the last two years of the simulation, the water content of C35/45 is the highest, C12/15 the lowest, and W/C=0.5 stands in between. This agrees with the vapor resistance of each concrete material. Lower vapor resistance results in higher drying capability.

2. Mold Index

Results of the mold VTT index for the Wall Assembly with three different concretes are provided in Table 5. "Very sensitive" is selected as the sensitivity class of the interior face of the inner concrete layer. The sensitivity class is set to "medium resistant" for the other monitoring point. The decline factor of mold is set to a relatively low decline (0.25) to have a more critical condition for simulations. Figures 24 and 25 show the mold index trend at monitor points.

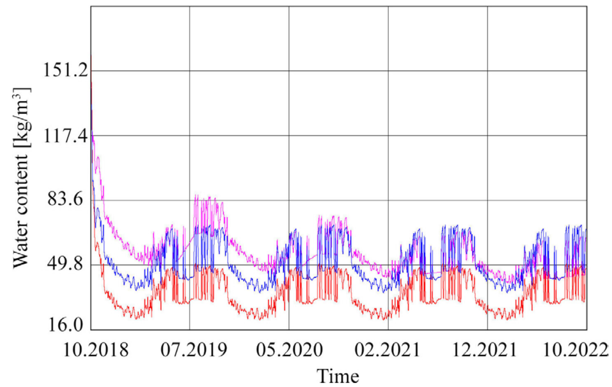

Figure 23 Water content of the inner concrete layer of Wall B.

Table 4 Mold index of Wall B with three different concretes.

Monitor point	**Mold Index**		
	C35/45	**C12/15**	**W/C 0.5**
The interior face of the inner concrete layer at the thermal bridge	0.456	0.55	0.312
The intersection of the insulation and the inner concrete layer	0.09	0.099	0.651

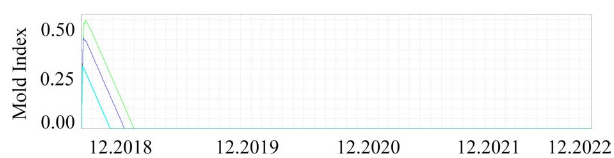

Figure 24 VTT mold index of the interior face of the inner concrete layer. C35/45 is blue, C12/15 is green, and W/C 0.5 is cyan.

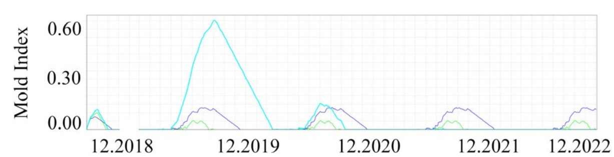

Figure 25 VTT mold index of the interior face of the inner concrete and insulation intersection. C35/45 is blue, C12/15 is green, and W/C 0.5 is cyan.

In both monitor positions, the mold index remains below three for all concrete types, within the threshold of the ASHRAE 160 requirements, suggesting no visible mold on the surface of the materials. The higher mold index of Wall B with "W/C = 0.5" is due to the longer drying time and higher moisture content in the first years of the simulation.

3. Corrosion

Figure 26 shows the 30-day hourly average relative humidity at the intersection of the insulation and the exterior concrete layer in Wall B with Rockwool as insulation and three types of concrete: C35/45, C12/15, and “W/C = 0.5”. Results show that the 30-day hourly average relative humidity is above 85% for the wall assemblies with C35/45 and C12/15 for the entire simulation period, which is more than the 80% threshold set by ASHRAE 160. In Wall B with “W/C = 0.5” concrete, it falls below the threshold in the last year. However, it is above 80% most of the time. Therefore, steel may corrode in all three assemblies.

4. Frost

Wall B with Rockwool and three different insulations were investigated. Figures 27 to 29 show the relative humidity and temperature graph for each assembly. Wall B with C35/45 rarely exceeds the 95% percent relative humidity threshold when the temperature falls below zero Celsius. Almost no frost risk is observed in Wall B with C12/15. In Wall B with “W/C = 0.5” concrete, there is a high risk of frost damage in the first years. However, in the last two years, it barely passed the threshold. Therefore, among these assemblies, W/C 0.5 has a high risk of frost damage in the first years till the initial moisture content dries.

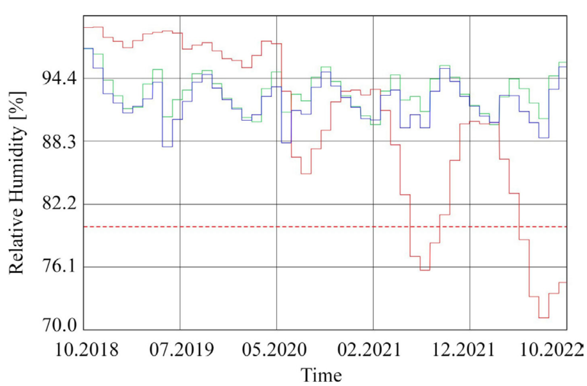

Figure 26 30-day hourly average Relative humidity of exterior concrete layer and insulation intersection in Wall B with C35/45 (blue), C12/15 (green), and W/C=0.5 (red).

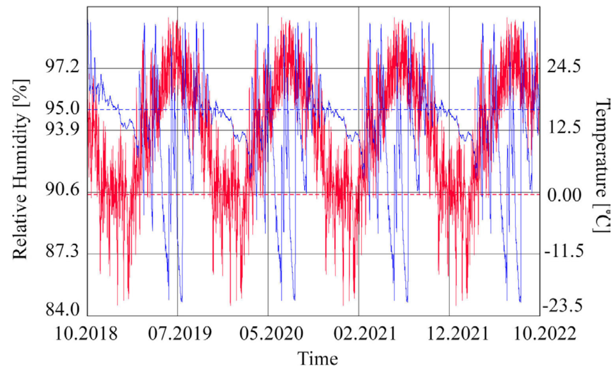

Figure 27 Relative humidity (blue) and temperature (red) for Wall B with C35/45 at the exterior concrete.

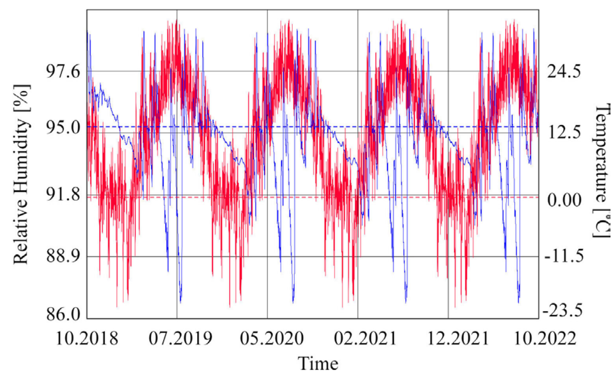

Figure 28 Relative humidity (blue) and temperature (red) for Wall B with C12/15 at the exterior concrete.

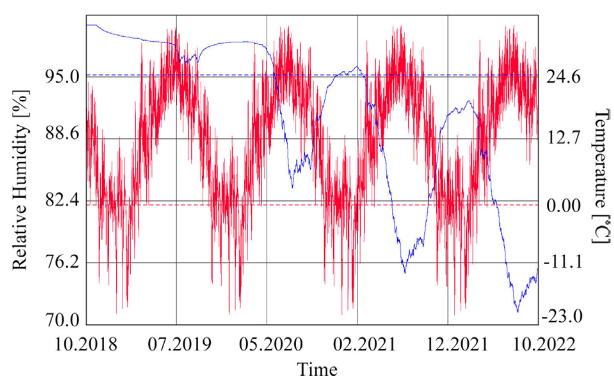

Figure 29 Relative humidity (blue) and temperature (red) for Wall B with “W/C = 0.5” at the exterior concrete layer.

Conclusion

This research investigated the hygrothermal performance of 3DCP wall assemblies with three different wall designs, four insulation materials, and three types of concrete.

- The investigations show that cellulose is not an ideal insulation material for 3D concrete printed walls due to the higher moisture content and not drying off the initial moisture content, leading to water accumulation and a high frost damage risk. Insulation materials with higher density or vapor resistance perform better with lower moisture content and frost damage risk.

- A comparison of different wall sections suggests that the wall designs without concrete connection bead between the interior and exterior concrete layers have lower water content.
- Evaluation of different concrete types suggests that less vapor resistance leads to the lower water content of the wall assemblies due to higher drying capability and thus lower frost damage risk.
- In all assemblies, steel components may corrode at the intersection of insulation and exterior concrete layer due to very high relative humidity.
- The mold index remains below ASHRAE's recommended thresholds for all simulated assemblies. Moreover, there are no indications of visible mold growth due to the high drying capability of assemblies and the high mold resistance of insulations and concrete.

This study is limited to the materials from the WUFI database and does not entirely represent various types of 3DCP wall properties or the material properties of the 3DCP as many of these remain proprietary. The simulation results are intended to provide insight into the potential risks of 3DCP projects regarding hygrothermal performances. Future work includes conducting field and laboratory tests to verify the simulation results by studying the moisture behavior of specimens based on real-world materials for 3DCP over the course of time.

Acknowledgment

This research is funded by the American Recovery & Reinvestment Act of 2009 (ARRA) as a grant from the Iowa Economic Development Authority and a Seed Grant from the Center for Global & Regional Environmental Research at the University of Iowa.

References

ASHRAE. 2021. 2021 ASHRAE® Handbook - Fundamentals (SI Edition) - 25. Heat, Air, and Moisture Control in Building Assemblies - Fundamentals (pp. 25.10). American Society of Heating, Refrigerating and Air-Conditioning Engineers, Inc.

ASHRAE 160. 2021. Criteria for Moisture-Control Design Analysis in Buildings (ANSI Approved) (160-2021). ASHRAE. Retrieved from https://www.ashrae.org/

ASTM International. 2023. ASTM E3054/E3054M-23, "Standard Guide for Characterization and Use of Hygrothermal Models for Moisture Control Design in Building Envelopes." West Conshohocken, PA. doi:10.1520/E3054_E3054M-23. Retrieved from www.astm.org.

Delgado, J., Ramos, N., Barreira, E., & Freitas, V. 2010. A critical review of hygrothermal models used in porous building materials. Journal of Porous Media, 13(3), 221-234. doi:10.1615/JPorMedia.v13.i3.30.

Glass, S., Kochkin, V., Drumheller, S., & Barta, L. 2015. Moisture Performance of Energy-Efficient and Conventional Wood-Frame Wall Assemblies in a Mixed-Humid Climate. Buildings, 5(3), 759–782. MDPI AG. Retrieved from http://dx.doi.org/10.3390/buildings5030759.

Glass, S., TenWolde, A., & Zelinka, S. 2013. Hygrothermal Simulation: A Tool for Building Envelope Design Analysis. Wood Design Focus, 23, 18-25.

Glass, S., & TenWolde, A. 2007. Review of In-Service Moisture and Temperature Conditions in Wood-Frame Buildings. Retrieved from https://www.researchgate.net/publication/305525050_Review_of_In-Service_Moisture_and_Temperature_Conditions_in_Wood-Frame_Buildings

Glass, S. V., Gatland, S. D., Ueno, K., & Schumacher, C. J. 2017. Analysis of Improved Criteria for Mold Growth in ASHRAE Standard 160 by Comparison with Field Observations. In Advances in Hygrothermal Performance of Building Envelopes: Materials, Systems, and Simulations (pp. 1-27). Retrieved from http://dx.doi.org/10.1520/STP159920160106.

Hukka, A., & Viitanen, H.A. 1999. A mathematical model of mould growth on wooden material. Wood Science and Technology, 33, 475-485

Jensen, N. F., Bjarløv, S. P., Rode, C., & Møller, E. B. 2020. Hygrothermal assessment of four insulation systems for interior retrofitting of solid masonry walls through calibrated numerical simulations. Building and Environment, 180, 107031. ISSN 0360-1323. doi:10.1016/j.buildenv.2020.107031.

Kaczorek, D. 2018. Hygrothermal assessment of internally insulated prefabricated concrete wall in Polish climatic condition. 12, 501-507. doi:10.1999/1307-6892/10008978. Retrieved from https://www.researchgate.net/publication/328601826_Hygrothermal_assessment_of_internally_insula ted_prefabricated_concrete_wall_in_Polish_climatic_condition

Krus, M., Kilian, R., & Sedlbauer, K. P. 2007. Mould growth prediction by computational simulation on historic buildings (pp. 185-189).

Künzel, H. M., Holm, A. H., & Krus, M. 2008. Hygrothermal Properties and Behaviour of Concrete.

Lepage, R., Schumacher, C., Knowles, W., & Glass, S. 2019. Biodeterioration Models for Building Materials: Critical Review. Journal of Architectural Engineering, 25. https://doi.org/10.1061/(ASCE)AE.1943-5568.0000366

Li, W., Pour-Ghaz, M., Castro, J., & Weiss, W. 2012. Water Absorption and Critical Degree of Saturation Relating to Freeze-Thaw Damage in Concrete Pavement Joints. Journal of Materials in Civil Engineering, 24, 299-307. doi:10.1061/(ASCE)MT.1943-5533.0000383.

Ojanen, T., Viitanen, H. A., Peuhkuri, R. H., Lähdesmäki, K., Vinha, J., & Salminen, K. 2010. Mold growth modeling of building structures using sensitivity classes of materials (pp. 1-10).

Overton, G. 2019. Hygrothermal performance of New Zealand Wall Constructions — meeting the durability requirements of the New Zealand Building Code. Canadian Journal of Civil Engineering, 46(11), 1063-1073. https://doi.org/10.1139/cjce-2018-0589

Pessoa, S., Jesus, M., Guimarães, A. S., Lucas, S. S., & Simões, N. (2023). Experimental characterisation of hygrothermal properties of a 3D printed cementitious mortar. *Case Studies in Construction Materials*, 19, e02355. https://doi.org/10.1016/j.cscm.2023.e02355

Straube, J., & Burnett, E. F. P. 2001. Overview of hygrothermal (HAM) analysis methods. In ASTM Moisture Control Manual (pp. 81-89).

Straube, J., & Schumacher, C. 2006. Assessing the durability impacts of energy efficient enclosure upgrades using hygrothermal modeling. Journal of the International Association for Science and Technology of Building Maintenance and Monuments Preservation, 2.

Straube, J., & Schumacher, C. 2007. Interior Insulation Retrofits of Load-Bearing Masonry Walls in Cold Climates. Journal of Green Building, 2(2), 42-50. doi:10.3992/jgb.2.2.42.

TenWolde, A. 2011. A Review of ASHRAE Standard 160—Criteria for Moisture Control Design Analysis in Buildings. Journal of Testing and Evaluation, 39(1), 77-81. https://doi.org/10.1520/JTE102896.

Vereecken, E., Vanoirbeek, K., & Roels, S. 2015. Towards a more thoughtful use of mould prediction models: A critical view on experimental mould growth research. Journal of Building Physics, 39, 102-123. doi:10.1177/1744259115588718.

Viitanen, H., Krus, M., Ojanen, T., Eitner, V., & Zirkelbach, D. 2015. Mold Risk Classification Based on Comparative Evaluation of Two Established Growth Models. Energy Procedia, 78, 1425-1430. doi:10.1016/j.egypro.2015.11.165.

WTA-Merkblatt 6-5-12/D. 2012. Innendämmung nach WTA-II: Nachweis von Innendämmungen mittels numerischer Berechnungsverfahren.

Wu. C., Doyle, S.D., Senske, N., & Evans, P. 2023. Energy Performance Simulation for 3D Concrete Printed Houses. Proceedings of Architectural Research Centers Consortium (ARCC) International Conference. Dallas, TX. April 12-15, 2023.

Wu. C., & Evans, P. 2024. An Integrated System for Improving 3D Concrete Printing Process. Proceedings of SimBuild Conference 2024. Denver, Colorado. May21-23, 2024. IBPSA.

Yu, S., Chang, S. J., Kang, Y., & Kim, S. 2016. Comparison of Hygrothermal Performance between Wood and Concrete Wall Structures using Simulation Program. Journal of the Korean Wood Science and Technology. The Korean Society of Wood Science Technology. https://doi.org/10.5658/wood.2016.44.2.283

Zelinka, S. L. 2013. Fastener Corrosion: A Result of Moisture Problems in the Building Envelope. Wood Design Focus, 23(3), 26-31.